HNUE JOURNAL OF SCIENCE
Journal of Natural Sciences, 2026, Volume 71, Issue 2, pp. 45-52
This paper is available online at https://hnuejs.edu.vn/ns
DOI: 10.18173/2354-1059.2026-0019

# STRUCTURAL PROPERTIES AND CRYSTALLIZATION OF DENSIFIED BORON SILICON NITRIDE: INSIGHTS FROM MOLECULAR DYNAMICS SIMULATION

Dinh Cong Thanh[1] and Le Van Vinh[2,*]
[1]*Phenikaa University Nano Institute (PHENA), Phenikaa University, Hanoi, Vietnam*
[2]*Phenikaa School of Computing, Phenikaa University, Hanoi, Vietnam*
[*]Corresponding author: Le Van Vinh, email: vinh.levan@phenikaa-uni.edu.vn

Received March 19, 2026. Revised May 26, 2026. Accepted June 30, 2026.

**Abstract.** We used molecular dynamics (MD) simulations to investigate the structural properties of boron silicon nitride (B-Si-N) under high pressure. The B-Si-N sample was cooled from 5000 K to 300 K at a constant pressure of 60 GPa. At 4000 K and 3500 K, the structure remained disordered. As the sample was cooled, a phase transition occurred between 3500 K and 3000 K. Common-neighbor analysis (CNA) showed that nitrogen atoms in the Si-N-rich region began to form crystalline clusters with face-centered cubic (FCC) and hexagonal close-packed (HCP) arrangements. Most clusters adopted FCC-like local ordering of nitrogen atoms, whereas a smaller fraction exhibited HCP ordering. The crystallization mechanism is discussed in detail.

***Keywords***: molecular dynamics, B-Si-N, crystallization, structural properties.

## 1. Introduction

In recent years, B-Si-N materials have attracted significant attention because of their high thermal stability, oxidation resistance, mechanical strength, and corrosion resistance [1]. B-Si-N is typically synthesized with an amorphous structure composed of slightly distorted $SiN_4$ tetrahedra and planar $BN_3$ units linked through shared nitrogen atoms, in which silicon and boron atoms are uniformly distributed [2]. This fully amorphous state can remain stable up to 1200 °C during annealing, but α-$Si_3N_4$ crystals appear once the annealing temperature reaches 1300 °C [3]. Experiments also show that the amorphous state remains stable up to 1600 °C [4] and even 1700 °C [5] in nitrogen environments, suggesting that crystallization in B-Si-N occurs over a range of temperatures. Both B-Si-N and $Si_3N_4$ have been synthesized under high-temperature and high-pressure conditions, with α-$Si_3N_4$ transforming completely into β-$Si_3N_4$ under compressive pressure. However, the presence of boron atoms hinders this transformation, and the α-$Si_3N_4$/β-

$Si_3N_4$ ratio increases with higher BN content in the samples [1]. Despite these findings, the crystallization mechanism of B-Si-N under high-temperature and compressive-pressure conditions remains unclear.

MD simulations have been widely used to investigate the structural properties of B-Si-N materials at the atomic scale [6]-[10]. Although boron atoms are bonded within the Si-N network, simulations have revealed the presence of Si-N–rich and B-N–rich regions [6], [9], [10]. In addition, simplex analysis has shown that B-Si-N materials contain distinct domains, including Si-N, B-N, and Si-B-N regions [9]. These findings raise important questions about how $Si_3N_4$ crystals form in Si-N-rich regions and how boron atoms influence the nucleation of $Si_3N_4$ crystals.

In this study, we use MD simulations to investigate both the structural properties and the crystallization process of B-Si-N materials. We simulated a B-Si-N sample at high temperature under compressive pressure and then cooled it to room temperature. During cooling, we analyzed the structural characteristics of the model to explore the nucleation pathway in B-Si-N.

## 2. Computational methods

We initially generated random atomic coordinates for the $BN_{25}(Si_3N_4)_{75}$ sample, containing 11,500 atoms in a simulation box measuring $56 \times 56 \times 56$ Å$^3$. We then applied the conjugate gradient algorithm to obtain a stable configuration with minimum energy. This configuration served as the input for the MD simulations. The simulations used the two-body empirical Marian–Gastreich potential because it is computationally efficient, produces models with relatively few coordination defects, and yields reasonable enthalpies of formation [8]. The parameters of this potential are reported elsewhere [11]. We integrated the equations of motion using the Verlet algorithm to simulate atomic trajectories and applied periodic boundary conditions to the simulation box. To control temperature and pressure, we used the Berendsen thermostat and barostat [12].

The sample was first heated in the NPT ensemble at 0 GPa and 5000 K for 100 ps. It was then cooled to 300 K at a pressure of 60 GPa at a cooling rate of 10 K/ps. To analyze the structure, we calculated the radial distribution function (RDF), examined structural units and linkages, and performed common-neighbor analysis (CNA) [13]. We defined the $SiN_x$ structural unit by placing the Si atom at the center and constructing a sphere with a radius of $r_{Si\text{-}cut\text{-}off} = 2.50$ Å, which corresponds to the first minimum of the Si–N pair RDF $g_{Si\text{-}N}(r)$. This sphere contained x N atoms. Similarly, we defined the $BN_y$ structural unit by placing the B atom at the center and using a cutoff radius of $r_{B\text{-}cut\text{-}off} = 1.91$ Å. For the $NSi_m$, $N(Si,B)_n$, and $NB_q$ linkages, we selected the N atom as the center of the corresponding spheres. Atomic configurations were visualized using OVITO software [14].

## 3. Results and discussion

Figure 1 shows the change in sample volume with decreasing temperature. The volume decreases sharply between 3500 K and 3000 K, indicating a phase transition. Previous experiments reported that the structural transformation from α-$Si_3N_4$ to γ-$Si_3N_4$ occurs at 4000 K under 45 GPa [15], while the transition from amorphous BN to cubic

BN occurs above 2473 K at 7.7 GPa [16]. These results suggest that the phase transition observed in B-Si-N more likely corresponds to crystallization of silicon nitride than to crystallization of boron nitride.

Figure 2 shows the changes in the RDFs with decreasing temperature. At 4000 K and 3500 K, the RDFs of Si–N, B–N, and N–N pairs display two peaks, with the main peak much more intense than the secondary peak, indicating a disordered structure. When the temperature drops below 3000 K, the pair RDFs ($g_{Si–N}(r)$, $g_{B–N}(r)$, and $g_{N–N}(r)$) exhibit additional, higher, and narrower peaks, suggesting that the structure becomes more ordered as the temperature decreases. At 4000 K, the main peaks of $g_{Si–N}(r)$, $g_{B–N}(r)$, and $g_{N–N}(r)$ are located at 1.74 Å, 1.41 Å, and 2.51 Å, respectively. As the temperature decreases, these peaks grow in intensity and shift slightly toward larger r values, indicating that the Si–N, B–N, and N–N bond lengths increase slightly. At 300 K, the main peaks are located at 1.82 Å, 1.47 Å, and 2.57 Å for Si–N, B–N, and N–N pairs, respectively. These values are close to experimental values for γ-$Si_3N_4$ [17], where the $Si–N_{tet}$, $Si–N_{oct}$, and N–N bond lengths are 1.7849 Å, 1.8718 Å, and 2.5539 Å, respectively, and for hexagonal BN [18], which has a B–N bond length of 1.45 Å.

Figure 3 shows how the fractions of structural units and linkages vary with decreasing temperature. For $SiN_x$ (x = 4, 5, and 6) units, the fractions of $SiN_4$ and $SiN_5$ decrease rapidly, while $SiN_6$ increases sharply between 3500 K and 3000 K, indicating a strong structural transition in this range. The $BN_3$ and $BN_4$ units display opposite trends: $BN_3$ decreases quickly from 4000 K to 3500 K, then rises sharply between 3500 K and 3000 K, and finally decreases gradually to 300 K, while $BN_4$ units show the opposite behavior.

For $NSi_m$ and $N(Si,B)_n$ linkages, which connect $SiN_x$ and $BN_y$ units, no $NB_q$ linkages were observed, indicating the absence of a B–N–rich region. At 3500 K, the fractions of $NSi_m$ and $N(Si,B)_n$ linkages are 75.56% and 24.44%, respectively. The $NSi_m$ linkages connect to form an extended network, whereas the N(Si,B)n linkages are clustered together, with the largest cluster containing about 94.15% of all $N(Si,B)_n$ linkages. Cross sections of these linkages are shown in Figure 4. Thus, interconnected Si–N–rich regions extend throughout the sample, whereas the mixed Si–B–N region consists mainly of clustered $N(Si,B)_n$ linkages.

As shown in Figure 3, $NSi_3$ and $NSi_4$ linkages decrease sharply, while $NSi_5$ and $NSi_6$ increase sharply between 3500 K and 3000 K. In contrast, $N(Si,B)_4$ linkages increase slightly, and $N(Si,B)_3$ linkages decrease slightly as the temperature decreases. These results indicate that the Si–N–rich region undergoes a strong structural change between 3500 K and 3000 K, while the mixed Si–B–N region evolves more gradually as the temperature decreases.

We performed CNA to detect crystalline structures in the sample and found that nitrogen atoms form both FCC and HCP sublattices. Figure 5 shows the fractions of FCC, HCP, and amorphous nitrogen atoms with decreasing temperature. No crystalline structures appeared above 3500 K. However, significant numbers of FCC and HCP nitrogen atoms formed at 3250 K. The fraction of FCC atoms increases rapidly between 3500 K and 2000 K and then grows more gradually at lower temperatures, whereas HCP atoms increase steadily throughout cooling. At 300 K, the sample contains 39.6% FCC, 5.8% HCP, and 54.6% amorphous nitrogen atoms.

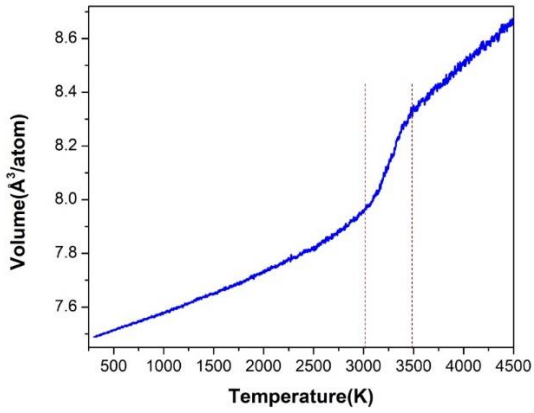


***Figure 1. Change in volume with decreasing temperature***

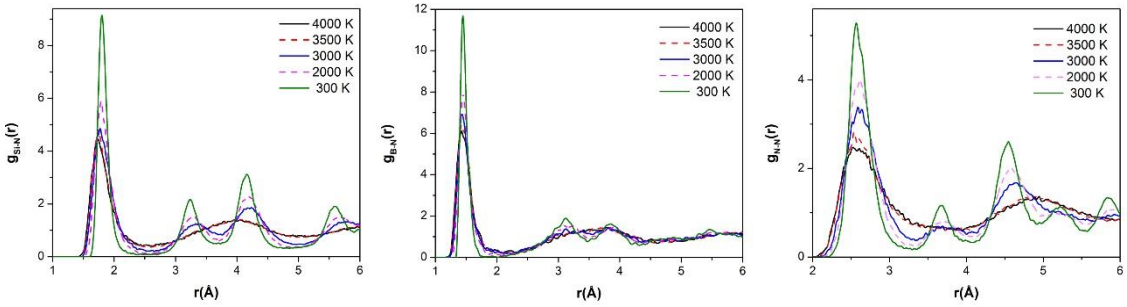


***Figure 2. Pair RDFs at different temperatures***

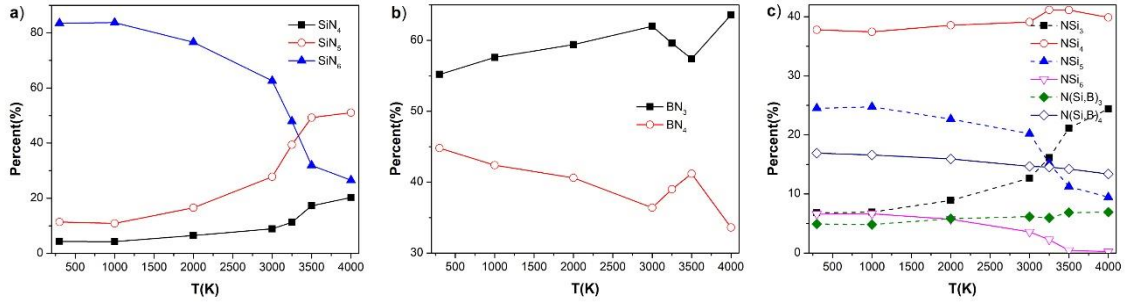


***Figure 3. Changes in the fractions of structural units and linkages with decreasing temperature***

At 3500 K, only 3 FCC and 1 HCP nitrogen atoms were observed, all of which were bonded to silicon. By 3250 K, the sample contained 584 FCC and 57 HCP nitrogen atoms. Of these, 11.47% of FCC atoms and 21.05% of HCP atoms were bonded to both silicon and boron, while the remainder were bonded exclusively to silicon. At 300 K, 12.73% of FCC atoms and 28.54% of HCP atoms were bonded to both silicon and boron. These results suggest that crystalline nucleation begins in the Si–N–rich region and then expands toward the mixed Si–B–N region. Figure 6 illustrates the atomic configurations at different temperatures, which show the growth of crystalline grains composed of FCC nitrogen atoms (green). HCP nitrogen atoms (blue) alternate with amorphous nitrogen atoms (red), while boron atoms (cyan) are distributed within the structure.

We calculated the average potential energies of FCC, HCP, and amorphous nitrogen atoms, as shown in Figure 7. FCC nitrogen atoms exhibit the lowest potential energy, followed by HCP atoms, while amorphous atoms have the highest. This trend indicates that nitrogen atoms tend to transform into the most stable state, which is the FCC structure. As illustrated in Figure 6, FCC-ordered structures form crystalline grains that are surrounded by HCP structures interspersed with amorphous regions, which act as grain boundaries. These amorphous regions arise from the incorporation of boron atoms into the Si–N network.

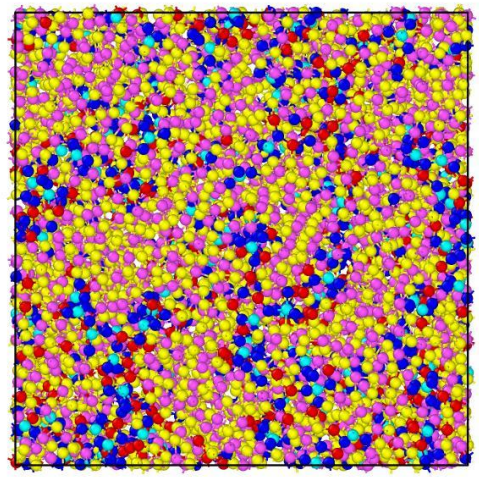

***Figure 4. Cross section of the sample at 3500 K (yellow: N atom belonging to $NSi_m$ linkage, blue: N atom belonging to $N(Si,B)_n$ linkage, pink: Si atom belonging to $NSi_m$ linkage, red: Si atom belonging to $N(Si,B)_n$ linkage, cyan: B atom belonging to $N(Si,B)_n$ linkage***

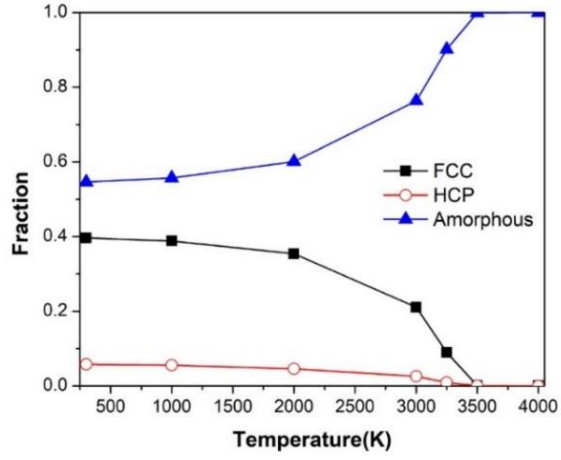


***Figure 5. Fractions of FCC, HCP, and amorphous nitrogen atoms with decreasing temperature***

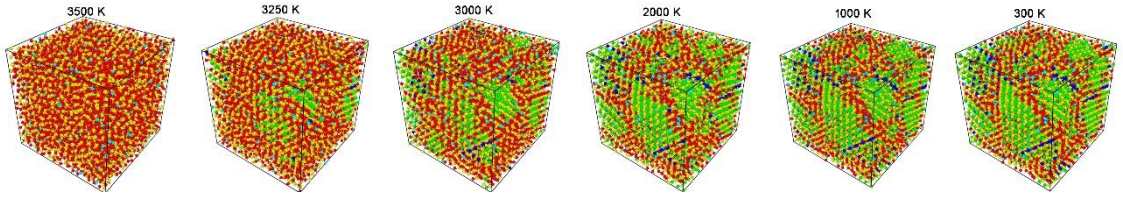


***Figure 6. Visualization of atoms with FCC and HCP ordering (green: FCC N atom, blue: HCP N atom, red: amorphous N atom, yellow: Si atom, and cyan: B atom)***

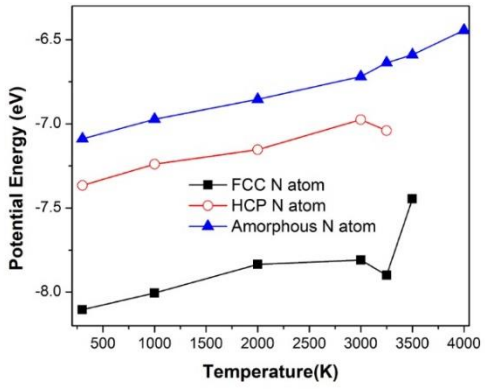


***Figure 7. Average potential energy of FCC, HCP, and amorphous nitrogen atoms with decreasing temperature***

## 4. Conclusions

We used MD simulations to study the structural properties and crystallization behavior of the $BN_{25}(Si_3N_4)_{75}$ sample. The sample was heated to a high temperature and then cooled to room temperature at a pressure of 60 GPa. Above 3500 K, the structure remained disordered, with $SiN_x$ and $BN_y$ units connected through $NSi_m$ and $N(Si,B)_n$ linkages. An Si–N–rich region formed and expanded throughout the sample, whereas no B–N–rich region was observed. Instead, mixed Si–B–N regions developed, with the largest $N(Si,B)_n$ cluster containing about 94.15% of all $N(Si,B)_n$ linkages. A phase transformation occurred between 3500 K and 3000 K, during which nucleation was dominated by FCC-like local ordering of nitrogen atoms, with a smaller fraction showing HCP-like local ordering. These nuclei formed initially in the Si–N–rich region, where FCC atoms exhibited the lowest potential energy, followed by HCP atoms and then amorphous atoms. As the temperature decreased, crystalline grains of FCC atoms grew, whereas a small number of HCP atoms were interspersed with amorphous Si–B–N structures, forming grain boundaries.

***Note for contributors:***

- Short bio: Dinh Cong Thanh is a PhD student at Phenikaa University Nano Institute (PHENA), Phenikaa University, Hanoi, Vietnam; Le Van Vinh is an Associate Professor at the Faculty of Information Systems, Phenikaa School of Computing, Phenikaa University, Hanoi, Vietnam.

- Authors' contributions: Dinh Cong Thanh: formal analysis, investigation, data curation, visualization, writing – original draft; Le Van Vinh: conceptualization, methodology, software, formal analysis, investigation, data curation, writing – review and editing, resources, supervision, validation.

***Conflict of interest:*** The authors declare no conflict of interest.

***Acknowledgments:*** The authors would like to thank Phenikaa University for its support for this research.

## REFERENCES

[1] W. Li, S. Ma, S. Cui, J. Ding, M. Widenmeyer, X. Zhang, Y. Zhan, Z. Yue, W. Zhang, P. Zhu, T. Cui, A. Weidenkaff & R. Riedel, "High-pressure synthesis, mechanical properties and oxidation behavior of advanced boron-containing α/β-Si3N4/Si ceramics using polymer-derived amorphous SiBN ceramics", *Journal of Advanced Ceramics*, vol. 13, no. 10, pp. 1611-1621, 2024. https://doi.org/10.26599/JAC.2024.9220961

[2] U. Muller, W. Hoffbauer & H. Jansen, "Short-Range Ordering in Amorphous Si3B3N7 As Determined by Multinuclear NMR Spectroscopy", *Chemistry of Materials*, vol. 12, no. 8, pp. 2341-2346, 2000. https://doi.org/10.1021/cm9911870

[3] X. Long, C. Shao & W. Wang, "Effects of boron content on the microwave-transparent property and high-temperature stability of continuous SiBN fibers", *Journal of the American Ceramic Society*, vol. 103, no. 8, pp. 4436-4444, 2020. https://doi.org/10.1111/jace.17151

[4] Y. Liu, K. Chen, S. Peng, Y. Cui, K. Han, M. Yu & H. Zhang, "Synthesis and pyrolysis mechanism of a novel polymeric precursor for SiBN ternary ceramic fibers", *Ceramics International*, vol. 45, no. 16, pp. 20172-20177, 2019. https://doi.org/10.1016/j.ceramint.2019.06.286

[5] Y. Tang, J. Wang, X. Li, Z. Xie, H. Wang, W. Li & X. Wang, "Polymer-Derived SiBN Fiber for High-Temperature Structural/Functional Applications", *Chemistry – A European Journal*, vol. 16, no. 22, pp. 6458-6462, 2010. https://doi.org/10.1002/chem.200902974

[6] N. Liao, W. Xue, H. Zhou & M. Zhang, "Effects of BN content on the structural and mechanical properties of a-SiBN ceramics", *International Journal of Materials Research*, vol. 104, no. 2, pp. 162-167, 2013. https://doi.org/10.3139/146.110851

[7] J. Al-Ghalith, A. Dasmahapatra, P. Kroll, E. Meletis & T. Dumitrica, "Compositional and Structural Atomistic Study of Amorphous Si-B-N Networks of Interest for High-Performance Coatings", *The Journal of Physical Chemistry C*, vol. 120, no. 42, pp. 24346-24353, 2016. https://doi.org/10.1021/acs.jpcc.6b07507

[8] A. Dasmahapatra & P. Kroll, "Computational study of impact of composition, density, and temperature on thermal conductivity of amorphous silicon boron nitride", *Journal of the American Ceramic Society*, vol. 101, no. 8, pp. 3489-3497, 2018. https://doi.org/10.1111/jace.15470

[9] N. T. Thao, C. D. Thanh, N. T. Trang & L. V. Vinh, "Structural properties and tensile deformation mechanism of amorphous Si3B3N7: Insights from molecular dynamics simulations", *Journal of Non-Crystalline Solids*, vol. 615, p. 122431, 2023. https://doi.org/10.1016/j.jnoncrysol.2023.122431

[10] M. Durandurdu, "Phase-separated amorphous Si2BN: A computational study", *Journal of Applied Physics*, vol. 137, no. 6, p. 065104, 2025. https://doi.org/10.1063/5.0244715

[11] C. M. Marian, M. Gastreich & J. D. Gale, "Empirical two-body potential for solid silicon nitride, boron nitride, and borosilazane modifications", *Physical Review B*, vol. 62, pp. 3117-3124, 2000. https://doi.org/10.1103/PhysRevB.62.3117

[12] H. J. C. Berendsen, J. P. M. Postma, W. F. van Gunsteren, A. DiNola & J. R. Haak, "Molecular dynamics with coupling to an external bath", *The Journal of Chemical Physics*, vol. 81, no. 8, pp. 3684-3690, 1984. https://doi.org/10.1063/1.448118

[13] D. Faken & H. Jonsson, "Systematic analysis of local atomic structure combined with 3D computer graphics", *Computational Materials Science*, vol. 2, no. 2, p. 279, 1994. https://doi.org/10.1016/0927-0256(94)90109-0

[14] A. Stukowski, "Visualization and analysis of atomistic simulation data with OVITO–The open visualization tool", *Modelling and Simulation in Materials Science and Engineering*, vol. 18, p. 015012, 2010. https://doi.org/10.1088/0965-0393/18/1/015012

[15] H. Yao, Q. Xu & J. Tang, "Synthesis and stability of cubic silicon nitride", *Advanced Materials Research*, vol. 79-82, p. 1467, 2010. https://doi.org/10.4028/www.scientific.net/AMR.79-82.1467

[16] H. Lorenz & I. Orgzall, "Influence of the initial crystallinity on the high pressure–high temperature phase transition in boron nitride", *Acta Materialia*, vol. 52, no. 7, pp. 1909–1916, 2004. https://doi.org/10.1016/j.actamat.2003.12.030

[17] J. Z. Jiang, K. Stahl, R. W. Berg, D. J. Frost, T. J. Zhou & P. X. Shi, "Structural characterization of cubic silicon nitride", *Europhysics Letters*, vol. 51, no. 1, p. 62, 2000. https://doi.org/10.1209/epl/i2000-00337-8

[18] S. Roy, X. Zhang, A. B. Puthirath, A. Meiyazhagan, S. Bhattacharyya, M. M. Rahman, G. Babu, S. Susarla, S. K. Saju, M. K. Tran, L. M. Sassi, M. A. S. R. Saadi, J. Lai, O. Sahin, S. M. Sajadi, B. Dharmarajan, D. Salpekar, N. Chakingal, A. Baburaj, X. Shuai, A. Adumbumkulath, K. A. Miller, J. M. Gayle, A. Ajnsztajn, T. Prasankumar, V. V. J. Harikrishnan, V. Ojha, H. Kannan, A. Z. Khater, Z. Zhu, S. A. Iyengar, P. A. d. S. Autreto, E. F. Oliveira, G. Gao, A. G. Birdwell, M. R. Neupane, T. G. Ivanov, J. Taha-Tijerina, R. M. Yadav, S. Arepalli, R. Vajtai & P. M. Ajayan, "Structure, Properties and Applications of Two-Dimensional Hexagonal Boron Nitride", *Advanced Materials*, vol. 33, no. 44, p. 2101589, 2021. https://doi.org/10.1002/adma.202101589